The effect of size and size distribution on the oxidation kinetics and plasmonics of nanoscale Ag particles

2010 Nanotechnology 21 215706

(http://iopscience.iop.org/0957-4484/21/21/215706)

Nanotechnology **21** (2010) 215706 (5pp) doi:10.1088/0957-4484/21/21/215706

The effect of size and size distribution on the oxidation kinetics and plasmonics of nanoscale Ag particles

Hua Qi, Dimitri Alexson, Orest Glembocki and S M Prokes

Electronics Science and Technology Division, Naval Research Laboratory, Washington, DC 20375, USA

E-mail: huaqi@ccs.nrl.navy.mil and Prokes@estd.nrl.navy.mil

Received 22 January 2010, in final form 16 April 2010
Published 30 April 2010
Online at stacks.iop.org/Nano/21/215706

Abstract

We employed a simple and effective electroless (EL) plating approach to produce silver nanoparticles (NPs) on bare silicon, on dielectric ZnO nanowires (NWs) and on Si NWs, respectively. The surface stability of the homogeneous Ag NPs formed on the ZnO NW surfaces was investigated by surface enhanced Raman spectroscopy (SERS), which show that the attachment of thiol to the Ag surface can slow down the oxidation process, and the SERS signal remains strong for more than ten days. To further examine the Ag NP oxidation process in air, the oxygen content in the silicon nanowire core/Ag sheath composites was monitored by the energy dispersive x-ray (EDX) method. The amount of oxygen in the system increases with time, indicating the silver NPs were continuously oxidized, and it is not clear if saturation is reached in this time period. To investigate the influence of the Ag NPs size distribution on the oxidation process, the oxygen amount in the NPs formed by EL deposition and e-beam (EB) evaporation on a bare silicon surface was compared. Results indicate a faster oxidation process in the EL formed Ag NPs than those produced by EB evaporation. We attribute this observation to the small diameter of the EL produced silver particles, which results in a higher surface energy.

(Some figures in this article are in colour only in the electronic version)

1. Introduction

There has been significant interest in a large variety of silver nanostructures due to their broad potential applications in catalysis [1–4], electronics [5, 6], material sciences [7, 8], biological action [9], and surface plasmon resonance (SPR) [10, 11]. Various approaches have been reported for the formation of silver nanostructures including wet chemical synthesis [12], physical sputtering [13], plasma deposition [14], and high-power ion beam irradiation [15]. It is well known that the extremely small nanostructures may lead to enhanced or novel properties when compared with the bulk material. In the case of silver nanoparticles, the extremely small sizes result in the particles having a large surface to volume ratio, which enhances their interaction with various molecular species and increases the possibility of surface functionalization for a number of applications. In recent years, pure silver structures, including nanowires [16, 17], nanoparticles [18–20] or nanoclusters [21, 22] have been widely studied in surface enhanced Raman spectroscopy (SERS), aimed at sensing applications. However, due to the inherent nature of silver, the Ag surface is easily oxidized in the air. Hence, it is important to understand the silver nanoparticle oxidation processes in order to optimize this material for various applications. Recently, Erol *et al* reported on the deleterious effect of oxygen on SERS, indicating the importance of understanding the silver oxidation effect on the SERS sensitivity for the development of ultrasensitive SERS-based detection [23]. In this work, we have investigated the atmospheric stability of the silver nanostructures formed by an electroless (EL) plating approach and e-beam (EB) evaporation technique, respectively. Specifically, the silver nanostructure oxidation process was monitored by energy dispersive x-ray (EDX) analysis and the effect on the SERS performance was

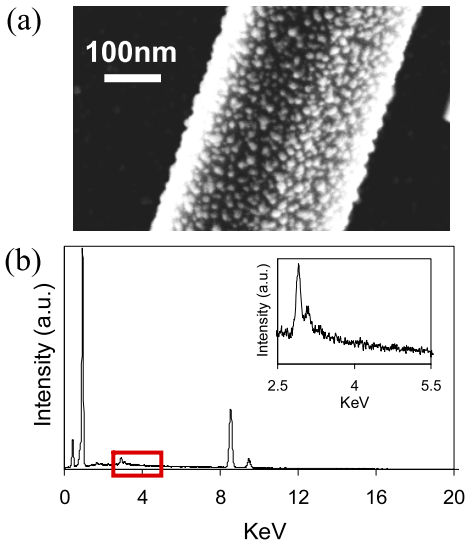

Figure 1. (a) SEM image of a dielectric ZnO NW core/Ag sheath composite produced by an electroless (EL) plating approach; (b) energy diffraction x-ray (EDX) spectra of the composites shown in (a); inset of (b) close-up plot of the silver EDX peak region (red rectangle).

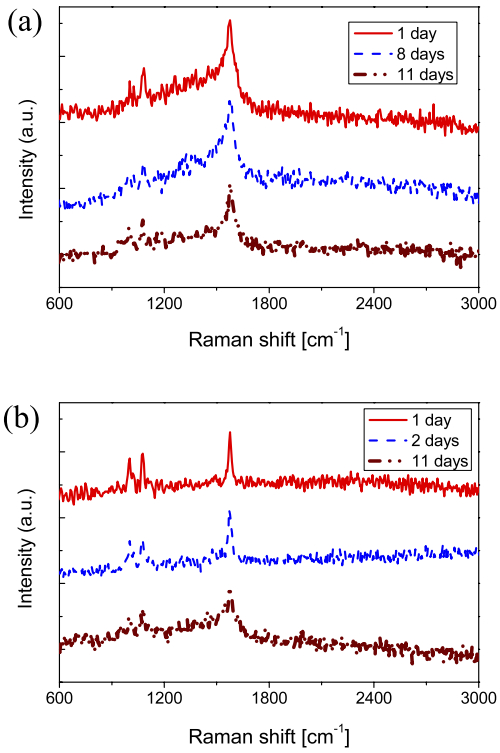

Figure 2. Surface enhanced Raman spectroscopy (SERS) on ZnO NW core/Ag sheath composites produced by (a) electroless (EL) plating, and (b) e-beam (EB) evaporation after prolonged exposure to air.

monitored using the Ag/Si system and Ag sheath/dielectric ZnO nanowires core composites.

2. Experimental details

The growth of ZnO NWs was performed via the vapor–solid (VS) growth mechanism at 560 °C for 30 min, using a Si(100) substrate, without a metal catalyst [24]. The silicon NWs were produced by a chemical wet etching process [25, 26]. The resulting Si NW arrays were sonicated in methanol and dropped on a bare silicon substrate. Silver nanostructures were formed by the EL silver plating process [27] and by EB evaporation on these NWs and on a bare silicon surface, using a FC-2000 Temescal E-beam evaporation system. Both EB and EL deposited silver structures deposited on the NWs and on the silicon were investigated using a LEO SUPRA 55 scanning electron microscope (SEM) with energy dispersive x-ray (EDX) capabilities. The EDX data were collected for 300 s at a voltage of 20 kV. Three locations were investigated on each sample surface, and the data were analyzed using the average absolute deviation from the median as error bars. The dielectric NW core/Ag sheath composites were further studied in SERS to investigate the oxidation process. The SERS measurements were carried out utilizing a confocal μ-Raman system which consisted of a Mitutoyo microscope and an Ocean Optics QE65000 spectrometer equipped with a thermoelectrically cooled CCD. The 514.5 nm line of an Ar ion laser was used as the excitation source. The microscope utilized a 100× 0.7 NA objective for focusing the laser light and was coupled to the spectrometer through a fiber optic cable. The spectra were collected with a low laser power of 0.75 mW on the sample.

3. Results and discussion

In the EL plating approach, a high density of 3D homogeneous silver nanoparticles (NPs) was formed on the ZnO NW surface, as shown in figure 1(a). The silver NPs on the NWs displayed a very narrow size distribution in the range of 10–30 nm, and strong SERS was obtained from these structures, due to the NP distribution on the curved NW surface. Figure 1(b) shows the EDX curve of the EL Ag covered ZnO NWs, and the inset is a close-up curve of the silver EDX peak region. The peaks at 1.03, 8.62 and 9.59 keV can be assigned to Zn [28, 29], and the weak features at 2.98 and 3.14 keV are attributed to Ag [30, 31]. This result confirms the deposition of silver particles on the NWs.

To examine the stability to oxidation of the silver nanoparticles, SERS measurements were carried out on a single dielectric ZnO nanowire core/silver sheath composite produced by both EL plating and EB evaporation approaches, and benzenethiol (BT) served as the SERS-active molecules. A single NW was randomly selected for SERS measurements and monitored for the signal strength from the moment that the composites were fabricated. Figures 2(a) and (b) show representative spectra which were obtained on both EL and EB generated nanowire/silver structures after the samples were exposed in air for several days. The major Raman peaks at 1002, 1071, and 1576 cm^{-1} can be assigned to the symmetric ring breathing mode, in plane C–H bending mode, and in plane C–C stretching mode of the phenyl ring of benzenethiol [32–37], respectively. In comparison with the

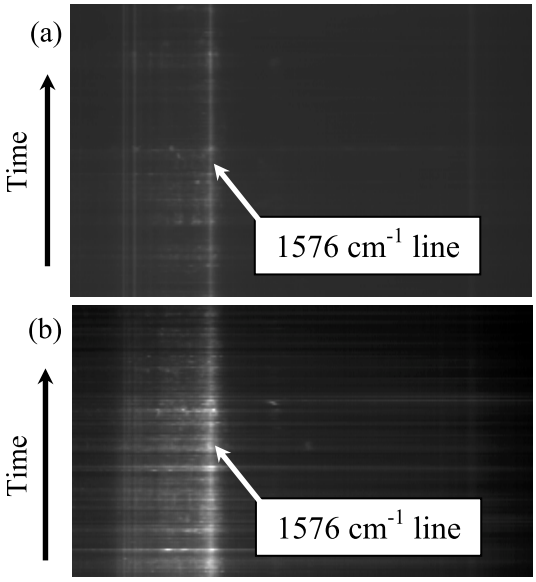

Figure 3. Time dependent behaviors of Ag on ZnO NW produced by (a) E-beam (EB), and (b) electroless (EL) depositions.

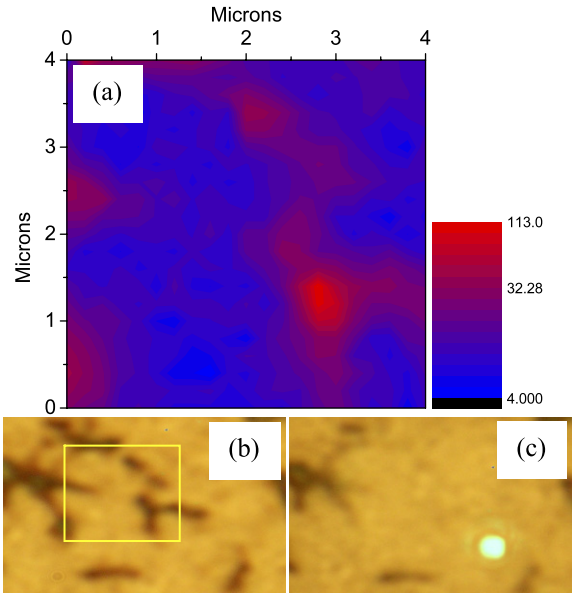

Figure 4. (a) Surface enhanced Raman spectroscopy (SERS) mapping of ZnO NWs core/silver sheath composites at the line of 1576 cm^{-1}; (b) and (c) microscope images before and after performing the mapping.

spectrum obtained on the first day, the intensity of the main SERS signal at 1576 cm^{-1} does not show a significant decrease as a function of time in the atmosphere, which implies that the thiol attachment to the Ag surface protects the silver from oxidation to a certain extent. To verify this point, a sample of ZnO NW/Ag composite was exposed in air for a week without the adsorption of BT, and then this sample was put into BT solution and used to measure its SERS behavior. Results show no obvious SERS signal. All these observations indicate the adsorption of BT could slow down the oxidation process of silver.

A large number of SERS measurements were performed on the newly prepared samples in order to investigate the time dependence behavior. We analyzed the effect of the power density used in the SERS experiments on the Ag nanoparticles, and specifically chose a laser power of 0.75 mW that was below any Ag damage threshold. As shown in figure 3, the main line of BT at 1576 cm^{-1} remained steady on both the e-beam and electroless silver covered NWs, indicating good stability of the freshly prepared silver sheath NWs under relatively short laser irradiation. However, once these structures were left in the atmosphere for longer times, SERS mapping of these structures suggested that the composites did gradually degenerate. Figure 4(a) shows SERS mapping results of the dielectric ZnO nanowire core/silver sheath composite at 1576 cm^{-1}, and its corresponding microscope images including before and after laser scanning (figures 4(b) and (c)). This sample was produced by the EL plating process, and the sample was kept in the air for eight days. The mapping region was 4×4 μm^2. As shown in the map, a strong SERS signal was obtained on the nanowire core/silver sheath composite region, while no SERS signal was observed on the bare silicon wafer (dark regions). However, exposure to the laser beam has led to the near disappearance of NW in the optical microscope (figures 4(b) and (c)), which can be attributed to the deterioration of the Ag coating, leading to a loss of contrast and visibility in the optical microscope. In fact, the NWs are just barely visible if viewed through the microscope eyepiece. When this sample was examined with AFM/TERS after mapping was finished, a complete loss of detectable SERS signal was noted. We attribute the loss of SERS signal to the Ag–S chemisorption bond cleavage due to the gradual oxidation of silver surface, which cause the BT molecules to desorb more easily under laser irradiation. This observation indicates that although initially the Ag is protected by the thiol layer, gradual oxidation in air does occur.

Since the dielectric ZnO NWs contain oxygen, it is difficult to monitor the change of oxygen content quantitatively. To further demonstrate the silver oxidation process in the air, we employed silicon NWs as the core, on which uniform, closely spaced silver NPs were deposited, using the EL Ag plated process as described above. As shown in the inset SEM image of figure 5, similar silver NP sizes and distributions on the Si NW was obtained, enabling direct comparison to the silver structures formed on the ZnO NWs. The oxygen amount in the EL produced Si NW core/Ag sheath system was monitored as a function of air exposure. The plot of the oxygen amount versus time shown in figure 5 clearly demonstrated that the amount of oxygen in the system increases with time, and it is not clear if the saturation is reached in this time period.

The small size usually means a large surface to volume ratio and a higher surface energy than the bulk. It has been well established that the oxidation rate of smaller particles is indeed greater than that of larger particles, such as in silicon and aluminum nanoparticles [38, 39]. Here we have also investigated the dependence of the silver oxidation process on the size of the NPs. In order to study the stability of a silver layer with a broad particle size distribution, Ag NPs

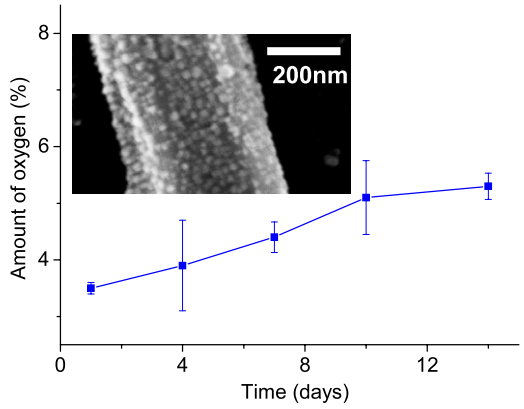

Figure 5. Plot of oxygen amount versus time on Si NW/Ag composite produced by EL plating; inset: SEM image of the EL silver plated Si NW.

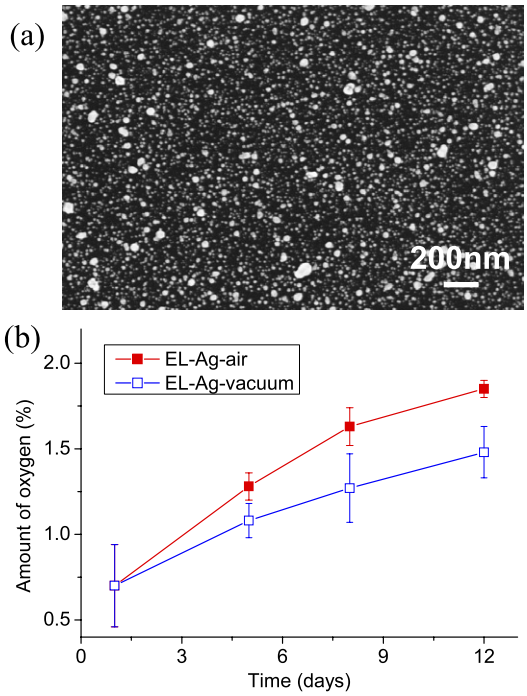

Figure 6. (a) SEM image of silver NPs on a silicon surface produced by electroless (EL) plating; (b) plot of oxygen amount versus time in the air (red) and in a plastic vacuum bag (blue).

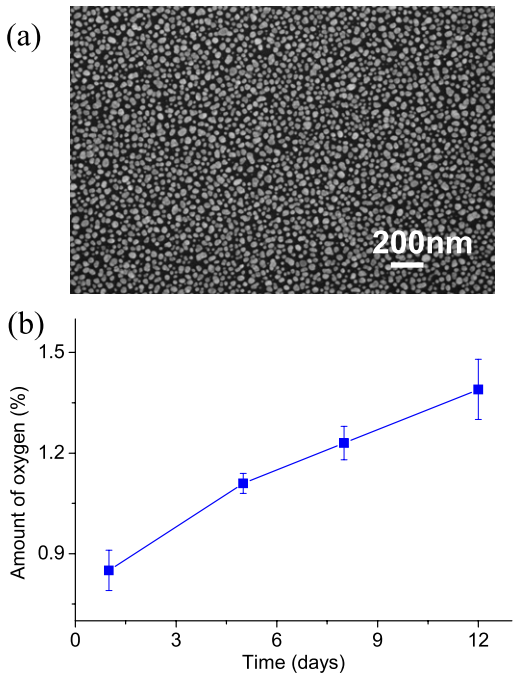

Figure 7. (a) SEM image of silver NPs on a silicon surface produced by e-beam (EL) deposition; (b) plot of oxygen amount versus time in the air.

were deposited on bare silicon via the EL chemistry process. This flat substrate exhibited a much broader size distribution in the range of 5–100 nm. We can not determine the thickness of these NPs by SEM and exactly calculate the surface area and surface energy, but the SEM images clearly indicates that most of the Ag NPs on NWs produced by EL had diameters in the ∼20 nm range. Additionally, we have analyzed the SEM images using ImageJ, which is a NIH program used for particle size analysis, and the average particle size obtained for the EL samples was on the order of 20 nm. A piece of the flat silicon covered with the EL plated silver NPs was cut into two pieces, which were separately stored in air and in moderate vacuum. Energy diffraction x-ray (EDX) analysis was again performed in order to obtain the silver oxidation rate. As shown in figure 6(b), it is obvious that the rate of oxidation is slower on the samples stored in the vacuum, compared to those stored in the air.

To further examine the dependence of the oxidation process on the silver NP size distribution, a layer of 6 nm of silver was deposited on a bare silicon piece by E-beam evaporation, at an evaporation rate of 1 Å s^{-1}. As shown in figure 7(a), the EB evaporated silver particle size was in the range of 15–55 nm, with a mean diameter of 35 nm. It should be noted that the oxidation rate of the EB produced silver (figure 7(b)) is slower than that formed by the EL chemical plating approach. This can be seen by comparing the results of figures 6(b) and 7(b), where the difference between those two curves increases with the time that the sample is exposed to air. These results suggest that the particle size, as well as the particle size distribution, can have a significant effect on the oxidation rate. However, it should be pointed out that although the EL produced silver particles oxidized somewhat faster, the advantage of this approach over the EB technique is that it could produce full coverage of any structures, regardless of the shape and orientation [27], which is not possible in the EB technique, since it is a 'line of sight' deposition process.

For the metal oxidation, it is well known that the idealized 'shrinking core' model is usually used to analyze the nanoparticle oxidation process [39]. In this model, the oxidation rate is dominated by two main steps, including the diffusion of oxygen through the oxide shell to the surface of the unreacted metal core, and the chemical reaction of oxygen with metal at unreacted core surface. With the thickness increase of the oxidized layer on particle surface, the oxidation rate is slowed down once the process becomes diffusion limited.

From the figures 5, 6(b) and 7(b), it is obvious that our observations are in good agreement with this model.

4. Summary

We have determined the stability of silver nanostructures by investigating the change of the amount of oxygen as a function of time in the atmosphere, using the Si/Ag system, produced via electroless (EL) plating and e-beam (EB) deposition. SERS measurements were also performed, and they show that a monolayer of benzene thiol can protect the silver surface for more than ten days. Our results also indicate that the sharp distribution of very small Ag NPs produced by EL show significantly enhanced oxidation rates compared to those formed by the EB technique. These results provide useful information on the silver nanostructure oxidation process which should be helpful in extending the silver lifetime for various applications.

Acknowledgments

This work was partially supported by the Office of Naval Research (ONR). HQ thanks the American Society for Engineering Education (ASEE) program. Ms Yung J is thanked for providing silicon NWs.

References

[1] Li J, Xu J, Dai W L and Fan K 2009 *J. Phys. Chem.* C **113** 8343
[2] Li W X, Stampfl C and Scheffler M 2003 *Phys. Rev. Lett.* **90** 256102
[3] Escosura-Muñiz A, Costa M M and Merkoçi A 2009 *Biosens. Bioeletron.* **24** 2475
[4] Dai J and Bruening M L 2002 *Nano Lett.* **2** 497
[5] Mukherjee B and Mukherjee M 2009 *Appl. Phys. Lett.* **94** 173510
[6] Peyser L A, Vinson A E, Bartko A P and Dickson R M 2001 *Science* **291** 103
[7] Gleiter H 2000 *Acta Mater.* **48** 1
[8] Musick M D, Keating C D, Lyon L A, Botsko S L, Peña D J, Holliway W D, McEvoy T M, Richardson J N and Natan M J 2000 *Chem. Mater.* **12** 2869
[9] Kumar A, Vemula P K, Ajayan P M and John G 2008 *Nat. Mater.* **7** 236
[10] Wang R C, Gao Y S and Chen S J 2009 *Nanotechnology* **20** 375605
[11] Wang N, Yang H F, Zhu X, Zhang R, Wang Y, Huang G F and Zhang Z R 2009 *Nanotechnology* **20** 315603
[12] Liang H, Yang H, Wang W, Li J and Xu H 2009 *J. Am. Chem. Soc.* **131** 6068
[13] Dowling D P, Betts A J, Pope C, McConnell M L, Eloy R and Arnaud M N 2003 *Surf. Coat. Technol.* **163** 637
[14] Jiang H, Manolache S, Wong A C L and Denes F S 2004 *J. Appl. Polym. Sci.* **93** 1411
[15] Kovivchak V S, Dubovik V I and Burlakov R B 2009 *J. Surf. Investig.-X-Ray Synchro.* **3** 268
[16] Aroca R F, Goulet P J G, dos Santos D S, Alvarez-Puebla R A and Oliveira O N 2005 *Anal. Chem.* **77** 378
[17] Encina E R, Perassi E M and Coronado E A 2009 *J. Phys. Chem.* A **113** 4489
[18] Fu X Q, Bei F L, Wu X D, Yang X J and Wang X 2009 *J. Mol. Struct.* **919** 7
[19] Mishra S, Singh R K and Ojha A K 2009 *Chem. Phys.* **355** 14
[20] Kim K, Kim K L and Lee S J 2005 *Chem. Phys. Lett.* **403** 77
[21] Šašić S, Itoh T and Ozaki Y 2005 *J. Raman Spectrosc.* **36** 593
[22] Saha S, Pal A, Pande S, Sarkar S, Panigrahi S and Pal T 2009 *J. Phys. Chem.* C **113** 7553
[23] Erol M, Han Y, Stanley S K, Stafford C M, Du H and Sukhishvil S 2009 *J. Am. Chem. Soc.* **131** 7480–1
[24] Prokes S M, Glembocki O J, Rendell R W and Ancona M G 2007 *Appl. Phys. Lett.* **90** 093105
[25] Zhang M L, Peng K Q, Fan X, Jie J S, Zhang R Q, Lee S T and Wong N B 2008 *J. Phys. Chem.* C **112** 4444
[26] Peng K, Yan Y, Gao S and Zhu J 2003 *Adv. Funct. Mater.* **13** 127
[27] Qi H, Alexson D, Glembocki O and Prokes S M 2010 *Nanotechnology* **21** 085705
[28] Liu S, Zhang H and Swihart M T 2009 *Nanotechnology* **20** 235603
[29] Büsgen T, Hilgendorff M, Irsen S, Wilhelm F, Rogalev A, Goll D and Giersig M 2008 *J. Phys. Chem.* C **112** 2412
[30] Gao Y, Shan D, Cao F, Gong J, Li X, Ma H, Su Z and Qu L 2009 *J. Phys. Chem.* C **113** 15175
[31] Chuang H Y and Chen D H 2009 *Nanotechnology* **20** 105704
[32] Jiang C, Lio W and Tsukruk V 2005 *Phys. Rev. Lett.* **95** 115503
[33] Ding J, Birss V and Liu G 1997 *Macromolecules* **30** 1442
[34] Sears W, Hunt J and Stevens J 1981 *J. Chem. Phys.* **75** 1589
[35] Zucolotto V, Ferreira M, Cordeiro M, Constantino C, Balogh D, Zanatta A, Moreira W and Oliveira O 2003 *J. Phys. Chem.* B **107** 3733
[36] Aroca R and Thedchanamoorthy A 1995 *Chem. Mater.* **7** 69
[37] Kim J H, Kang T, Yoo S M, Lee S Y, Kim B and Choi Y K 2009 *Nanotechnology* **20** 235302
[38] Yang D, Gillet J, Meunier M and Sacher E 2005 *J. Appl. Phys.* **97** 024303
[39] Park K, Lee D, Rai A, Mukherjee D and Zachariah M R 2005 *J. Phys. Chem.* B **109** 7290